Mecánica Computacional Vol. XXI, pp. 605–619
S. R. Idelsohn, V. E. Sonzogni and A. Cardona (Eds.)
Santa Fe–Paraná, Argentina, October 2002

NUMERICAL STUDY OF A THREE-PHASE SYSTEM: A METALLURGICAL LADLE

Carlos G. Méndez, Norberto Nigro and Alberto Cardona

CIMEC (INTEC), UNL-Conicet, Güemes 3450, 3000 Santa Fe, Argentina.
e-mail: cgmendez@ceride.gov.ar

Key Words: Multiphase flow, stirred ladle, non-drag forces.

Abstract. *From an industrial point of view, knowledge of flow conditions in a metallurgical ladle is of fundamental importance for optimization of refining process. Three different phases coexist in the ladle: two liquid phases, the molten metal and the slag, and a gaseous phase, the argon injected through a nozzle located at the bottom of the ladle. The dispersed gas phase induces a recirculating flow in the metal and generates turbulence in the plume region. As a consequence of buoyancy, the slag has a tendency to stratify above the metal, but there is also entrainment caused by the metal flow. Understanding flow conditions in the slag region will help in the comprehension of various phenomena such as mixing, slag emulsification, and chemical reactions between phases. To avoid difficulties due to operating conditions, a water-air scaled physical model is frequently used to simulate the argon and the metal (water and molten steel have similar kinematic viscosity), and the slag is modelled using oil or kerosene. Since there are much more experimental data for water-air models, we start simulating numerically this class of systems. In particular, we analyzed the experimental data obtained by Castillejos and Brimacombe*. Numerical calculations were made using the commercial code CFX. This program can predict the flow in a turbulent multiphase system and allows us to establish which are the most important physical phenomena that determine the behavior of the main variables in a metallurgical ladle. We analyze which are the governing equations that properly describe the system and present a detailed study of the water-air system. In addition, we show how the principal characteristics of the flow are modified when the free surface and the slag are incorporated into the model. The results obtained compare very well with experimental measurements and this suggests that the effects included in the model are the most relevant in order to suitably represent the ladle for technological purpose.*
** A. H. Castillejos and J. K. Brimacombe, Metall. Trans., 18B, 659 (1987).*

1 INTRODUCTION

Three different phases coexist in the refining operations in a metallurgical ladle: the molten metal, the slag and the argon injected to induce the stirring. Knowledge of the flow conditions of the metal, particularly in the region where it is in contact with slag, is very important for the industry. This information helps in the understanding of various phenomena such as mixing, slag emulsification in the molten metal phase, and chemical reactions between phases. Due to the high temperature operation conditions, direct measurements of flow conditions in the ladle are hard to implement. For this reason, a physical model of air and water is frequently used to simulate the real system.[1]

We simulated the water-air system numerically using the commercial code CFX-4.4. This is a program for the prediction of laminar and turbulent flow, and heat transfer, which includes features like multi-phase flow, combustion and particle transport. Flow calculations in this software are based on the resolution of the Navier-Stokes equations in either transient or stationary regimes. The code can solve free surface problems where the grid moves to fit the free surface depending upon an assumed boundary condition of constant pressure. An arbitrary number of phases may be specified. Phases are assumed to form an inter-penetrating continuum whereby each phase occupies a certain volume fraction of each control cell.

In this paper we analyze the effects that have to be included in the model in order to properly describe this industrial process for optimization. We will limit our analysis to the water-air system and the experiment we modelled is that of Ref. [2].

2 BALANCE EQUATIONS

Since we are only interested in a rather global information about gas phase, e.g. bubble velocity and concentration, and not in how a bubble is deformed, and since the length scale we want to resolve is larger than the scale in which phases are mixed, we chose an Eulerian-Eulerian approach to describe the system. In this formulation each phase is treated as an interpenetrating continuum, i.e., each phase is assumed present in each control volume, and assigned a volume fraction equal to the occupied fraction of the control volume.

Large bubbles can have a different velocity field from that of the continuous phase. In this case each phase have its own movement equation and the interaction between phases has to be modelled. This is the regime in which we are interested which is best described by the so-called multi-fluid model: a separate solution field exists for each phase and transported quantities interact via inter-phase transfer terms. Phases may have different velocities, but they will have a tendency to equalize because of inter-phase forces. Therefore, balance equations consist of equations corresponding to separate one-phase systems plus some additional terms that take into account their interaction.

We label phases by Greek indices α, β, γ, ... and denote the number of phases by N_P and the volume fraction of each phase by r_α. In the incompressible case, the balance

equations are[3]

$$\frac{\partial r_\alpha}{\partial t} + \nabla \cdot (r_\alpha \mathbf{U}_\alpha) = 0 \ , \tag{1}$$

$$\rho_\alpha \frac{\partial (r_\alpha \mathbf{U}_\alpha)}{\partial t} + \rho_\alpha \nabla \cdot (r_\alpha \mathbf{U}_\alpha \mathbf{U}_\alpha) - \nabla \cdot (r_\alpha \mu_\alpha (\nabla \mathbf{U}_\alpha + (\nabla \mathbf{U}_\alpha)^T)) = r_\alpha (\mathbf{B}_\alpha - \nabla p_\alpha) + \sum_{\beta=1}^{N_P} c_{\alpha\beta}^{(d)} (\mathbf{U}_\beta - \mathbf{U}_\alpha) + \mathbf{F}_\alpha \ , \tag{2}$$

$$\sum_{\alpha=1}^{N_P} r_\alpha = 1 \ , \tag{3}$$

$$p_\alpha = p_1 = p \ , \quad 2 \leq \alpha \leq N_P \ , \tag{4}$$

where $\mathbf{U}$ denotes velocity, ρ density, μ viscosity, $\mathbf{B}$ body forces, and p pressure. Terms containing coefficients $c_{\alpha\beta}^{(d)}$ are the inter-phase *drag forces* and the terms $\mathbf{F}_\alpha$ are any other inter-phase *non-drag forces*.

3 TURBULENCE IN TWO-PHASE FLOW

The subject of multi-phase turbulence modelling is not as well developed as single-phase turbulence modelling. There is no "industrial standard" model, like the single phase k–ε model which is known to perform reasonably well to engineering accuracy in a wide range of applications. Therefore, the model adopted is the simplest possible generalization of the single-phase k–ε model to the multi-phase situation, with the only modification being the possible inclusion of Sato's model for bubble induced turbulence.

3.1 The multi-fluid k–ε model

In the simple unmodified multi-fluid k–ε model, individual phases are allowed to be declared as turbulent or laminar. We assume that the eddy viscosity hypothesis holds for each turbulent phase: molecular and turbulent diffusion of momentum is governed by an effective viscosity

$$\mu_{\alpha eff} = \mu_\alpha + \mu_{T\alpha} \ , \tag{5}$$

where

$$\mu_{T\alpha} = C_\mu \rho_\alpha \frac{k_\alpha^2}{\varepsilon_\alpha} \ . \tag{6}$$

Thus, the equations for the turbulent incompressible case are

$$\frac{\partial r_\alpha}{\partial t} + \nabla \cdot (r_\alpha \mathbf{U}_\alpha) = 0 \ , \tag{7}$$

$$\rho_\alpha \frac{\partial(r_\alpha \mathbf{U}_\alpha)}{\partial t} + \rho_\alpha \nabla \cdot (r_\alpha \mathbf{U}_\alpha \mathbf{U}_\alpha) - \nabla \cdot (r_\alpha \mu_{\alpha eff} (\nabla \mathbf{U}_\alpha + (\nabla \mathbf{U}_\alpha)^T)) = r_\alpha (\mathbf{B}_\alpha - \nabla (p_\alpha + \frac{2}{3} \rho_\alpha k_\alpha)) + \sum_{\beta=1}^{N_P} c_{\alpha\beta}^{(d)} (\mathbf{U}_\beta - \mathbf{U}_\alpha) + \mathbf{F}_\alpha \ , \quad (8)$$

$$\sum_{\alpha=1}^{N_P} r_\alpha = 1 \ , \quad (9)$$

$$p_\alpha = p_1 = p, \quad 2 \leq \alpha \leq N_P \ , \quad (10)$$

together with the equations for k and ε, which are practically the same as those corresponding to single phase case.

$$\rho_\alpha \frac{\partial(r_\alpha k_\alpha)}{\partial t} + \rho_\alpha \mathbf{U}_\alpha \cdot \nabla (r_\alpha k_\alpha) - \nabla \cdot \left(\left(\mu + \frac{\mu_{T\alpha}}{\sigma_k} \right) r_\alpha \nabla k_\alpha \right) = r_\alpha (P_\alpha - \rho_\alpha \varepsilon_\alpha) + \sum_{\beta=1}^{N_P} c_{\alpha\beta}^{(k)} (k_\beta - k_\alpha) \ , \quad (11)$$

and

$$\rho_\alpha \frac{\partial(r_\alpha \varepsilon_\alpha)}{\partial t} + \rho_\alpha \mathbf{U}_\alpha \cdot \nabla (r_\alpha \varepsilon_\alpha) - \nabla \cdot \left(\left(\mu + \frac{\mu_{T\alpha}}{\sigma_\varepsilon} \right) r_\alpha \nabla \varepsilon_\alpha \right) = C_1 \frac{\varepsilon_\alpha}{k_\alpha} P_\alpha - C_2 \rho_\alpha \frac{\varepsilon_\alpha^2}{k_\alpha} + \sum_{\beta=1}^{N_P} c_{\alpha\beta}^{(\varepsilon)} (\varepsilon_\beta - \varepsilon_\alpha) \ , \quad (12)$$

where the shear production P_α is

$$P_\alpha = \mu_{eff} \nabla \mathbf{U}_\alpha : (\nabla \mathbf{U}_\alpha + (\nabla \mathbf{U}_\alpha)^T) \ . \quad (13)$$

The constants used are $C_\mu = 0.09$, $C_1 = 1.44$, $C_2 = 1.92$, $\sigma_k = 1.0$, $\sigma_\varepsilon = 1.22$. The only difference with the single phase case is the inclusion of the terms $\sum_{\beta=1}^{N_P} c_{\alpha\beta}^{(k)} (k_\beta - k_\alpha)$ and $\sum_{\beta=1}^{N_P} c_{\alpha\beta}^{(\varepsilon)} (\varepsilon_\beta - \varepsilon_\alpha)$, that interchange k and ε between the phases; however, since in our case we are modelling water as turbulent and air as laminar these interchange terms are zero.

4 NUMERICAL MODELLING

The numerical results were obtained solving a system with the following characteristics:

- Two dimensional with axial symmetry.

- Grids of 40x25, 80x50 and 160x100 rectangular elements.
- Isothermal and incompressible flow.
- Liquid phase (water) continuum and turbulent (k-e model).
- Gas phase (air) dispersed and laminar that can flow through the free surface.
- Air density depends only on hydrostatic pressure.
- Each phase has its own set of variables (multi-fluid model).
- Drag as well as non-drag forces are included.
- Deformable free surface.

The way in which the gas is dispersed in the ladle is governed by the buoyant force and by the interaction with the liquid phase. The interaction between phases is due mainly to drag forces which are originated by pressure and friction between phases and act in the direction opposite to movement. However, not only drag forces but also non-drag forces are important and have to be considered in this case. They are the *virtual mass force*, the *lift force*, and the *turbulent dispersion force*.

The virtual mass force represents the force due to the inertia of a bubble, including the surrounding liquid, when the bubble is accelerated. The lift force appears because a bubble moving in a linear shear flow has an unsymmetrical pressure distribution on its external boundary and then it is driven into the direction of largest relative velocity. The lift force, therefore, acts perpendicular to the relative velocity. When the typical size of the dispersed phase is of the order of the fluctuation length scale of the continuous phase, the effect of diffusion should be considered. In the laminar case this situation appears only when the phases are mixed at molecular level, which is not our case. However, when the flow regime is turbulent, fluctuations of the continuous phase may be comparable with the bubble size and diffusion may be important. This effect is usually taken into account through a non-drag force called turbulent dispersion force, but other alternatives exist as we will comment further on. Another effect that have to be taken into account is the turbulence that can be generated behind the bubbles. This effect can transform a laminar flow in a turbulent one or can increase an existing turbulence in the continuous phase.

All the effects mentioned are always present, although the relative importance of each one depends on the size of the bubbles and on the degree of turbulence in the system. In the literature, the drag force is always included to describe the interaction between the phases, but sometimes some or all of the other effects are neglected. Our results indicate that if we are interested in determining the velocity field of the liquid phase, we may use drastic approximations of this kind; however, in order to properly describe the gas velocity and volume fraction, non-drag forces have to be considered. Having a good description not only of the velocity field of the continuous phase but also of the volume

fraction of the dispersed phase will be of utmost importance in the description of the slag emulsification phenomena.

We will start showing preliminary results, including non-drag effects, of one of the cases studied in Ref. [2]. After that, will describe in more detail the way in which non-drag effects are implemented as well as how the numerical results can be improved when the influence of each effect is known.

In figure 1, streak lines representing the water velocity field and the air volume fraction are shown. This case corresponds to a cylindric ladle with internal diameter of 500 mm and height of water of 400 mm. The nozzle, with a diameter of 6.35 mm was located at the center of the bottom of the ladle and the gas flow rate was 371 cm^3/s at STP. There, we can see how the air injected at the bottom of the ladle induce a recirculating flow in the water.

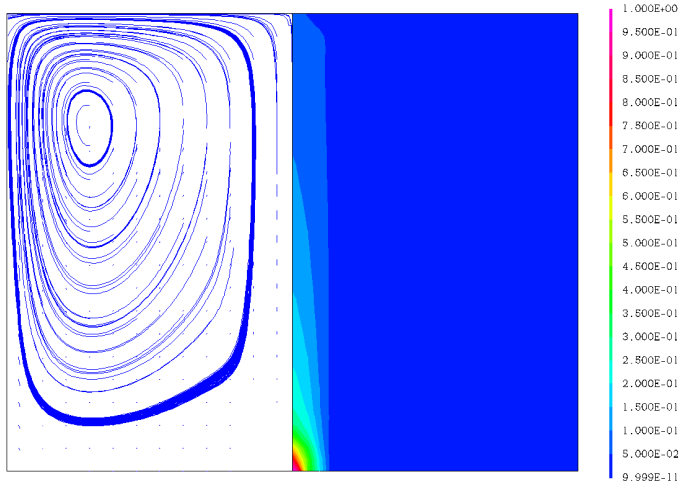

Figure 1: Streak lines corresponding to the water phase (left) and volume fraction of the air phase (right)

The volume fraction of the air on the symmetry axis of the cylinder as a function of vertical distance from the nozzle is shown in figure 2. We can see changes in the numerical predictions when non-drag effects with typical coefficients are included.

Gas fraction on figure 2 is a good indicator in order to see if the dispersed phase is correctly treated. If we have a good description of the volume fraction as a function of height on the symmetry axis, the radial dependency will also be well described because the gas flow rate is the same at any height. Consequently, lower gas volume fractions on the symmetry axis correspond to more dispersed volume fractions in the radial direction.

It is observed experimentally that after a given height from the nozzle, gas volume fractions have a similar behavior even when gas flow rate, diameter of the nozzle and bath depth are changed.

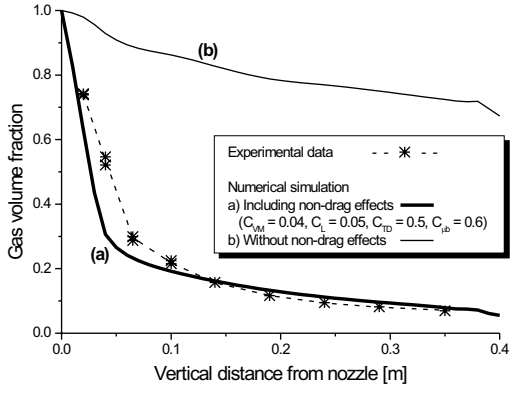

Figure 2: Volume fraction of the air phase on the symmetry axis of the ladle.

When results are shown as in figure 2, comparison with experimental results seems to be good at a first glance. However, when results are plotted in a log-log graphic like in figure 5 of Ref. [2], things do not look so favorable (see figure 3) even including non-drag effects.

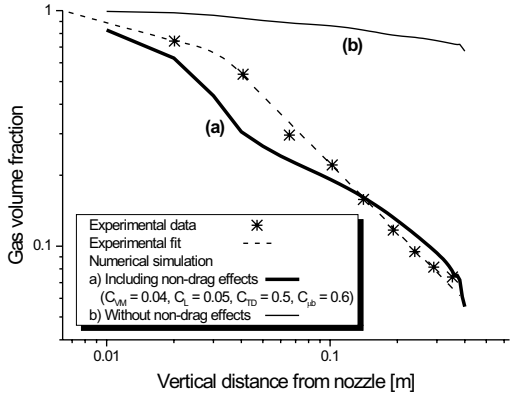

Figure 3: Volume fraction of the air phase on the symmetry axis of the ladle in a log-log graphic.

One of the weak points in the results of figure 3 is the difference with experiments near the nozzle. This region is hard to be described correctly because bubbles are large and

breakup and coalescence phenomena are important in this zone. Good modelling of these phenomena requires the consideration of bubbles of different sizes and is beyond the scope of this work (we are working with only one bubble size). Our primary interest is not in the region near the nozzle but in the region in which the plume is completely developed and where the bubble size distribution is more stable. As it can be seen in figure 3, the main problem in the developed plume region is that numerical and experimental gas fraction curves have different slopes. The slope of the gas fraction curve is a characteristic of the system that is maintained in different plumes (see, e.g., fig. 5 of Ref. [2]) and it should be desirable to reproduce this feature in numerical simulations. As we will show in what follows, even when working with a unique bubble size, the gas fraction can be well described when the influence of non-drag effects is taken into account.

4.1 Drag Force

In order to restrict the study to the non-drag forces, we will consider the same expression for the drag force in all cases. The total drag per unit volume in the continuous phase is usually written as

$$\mathbf{D}_{\alpha\beta} = c_{\alpha\beta}^{(d)}(\mathbf{U}_\beta - \mathbf{U}_\alpha) \; . \tag{14}$$

where

$$c_{\alpha\beta}^{(d)} = \frac{3}{4}\frac{C_D}{d} r_\beta \rho_\alpha \left|\mathbf{U}_\beta - \mathbf{U}_\alpha\right| \; . \tag{15}$$

For a particle of a given shape undergoing motion in a Newtonian incompressible fluid, C_D depends only on Reynolds number

$$Re = \frac{\rho_\alpha U d}{\mu_\alpha} \; , \tag{16}$$

where μ_α is the molecular viscosity of the continuous phase. The function $C_D(Re)$ may be determined experimentally, and is known as the *drag curve*. One of the most used drag coefficient, although not completely realistic for bubbles, corresponds to the drag experimented by a rigid and isolated sphere and is known as the *standard drag curve*. There are several empirical expressions for this curve, depending on the flow Reynolds number. One expression frequently used is that due to Schiller and Nauman[4]

$$C_D = \frac{24}{Re}(1 + 0.15 Re^{0.687}) \; , \tag{17}$$

which is valid in the range $0 \leq Re \leq 1000$. This is the expression for C_D that we will use in this work.

4.2 Non-Drag Forces

Virtual Mass: The virtual mass force accounts for the effect of acceleration of the liquid displaced by the bubbles, and can be modelled as

$$\mathbf{F}_\alpha^{VM} = r_\beta \rho_\alpha C_{VM} \left(\frac{D_\beta \mathbf{U}_\beta}{Dt} - \frac{D_\alpha \mathbf{U}_\alpha}{Dt} \right) \; . \tag{18}$$

Operators $D_{\alpha,\beta}/Dt$ denote the material derivatives corresponding to each phase. The coefficient C_{VM} is equal to 0.5 for individual spherical particles, but for bubbles its value is much more lower. In our study we consider values of C_{VM} up to 0.06.

In figure 4 we can see how the gas volume fraction is changed when the virtual mass coefficient is varied. As it is expected, the inclusion of this force affects the gas volume fraction mainly in the region near the nozzle where relative accelerations between phases are larger.

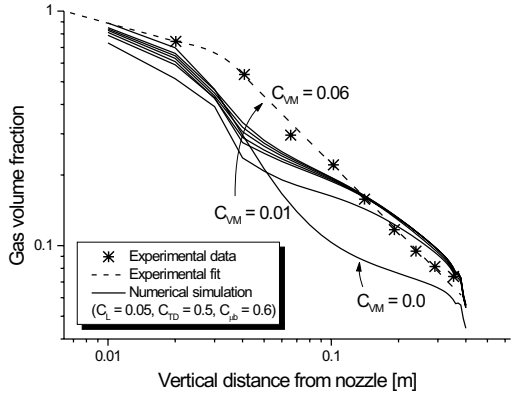

Figure 4: Axial gas fractions for different virtual mass coefficients

Lift: This force is given in terms of the slip velocity and of the curl of the continuous phase velocity by

$$\mathbf{F}_{\alpha}^{L} = r_{\beta}\rho_{\alpha}C_{L}(\mathbf{U}_{\beta} - \mathbf{U}_{\alpha}) \times (\nabla \times \mathbf{U}_{\alpha}) \; . \tag{19}$$

Here C_L is 0.5 for inviscid flow around a sphere, but it can take values as lower as 0.01 for viscous flow.

In figure 5 we can see that a variation of the lift coefficient affects the values of the volume fraction in the whole height of the bath. Also, the slope of the curve in a log-log graphic is modified.

Recent studies indicate that C_L depends on the Eötvös number and can take even negative values for large bubbles.[5] This is an important fact that should be taken into account if bubbles of different sizes are considered.

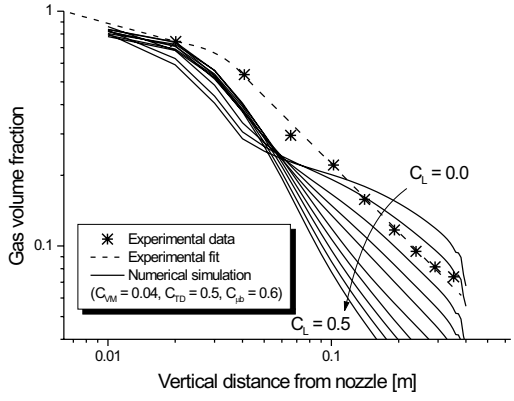

Figure 5: Axial gas fractions for different lift coefficients

Turbulent dispersion force: This force appears as a consequence of the increment of diffusion due to turbulence. Since it is related with diffusion, it seems natural to incorporate this effect as a diffusive term in the continuity equation as in Ref. [6]. However, we preferred to model this phenomenon including a force in the moment equation,[7] because in this way, the contribution due to diffusion is included in the velocity variable.

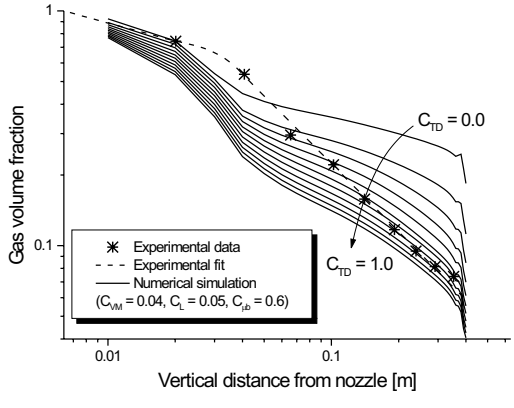

Figure 6: Axial gas fractions for different turbulent dispersion force coefficients

The expression that we used for the turbulent dispersion force is

$$\mathbf{F}_\alpha = -C_{TD}\rho_\alpha k_\alpha \nabla r_\alpha \ , \tag{20}$$

where C_{TD} is a parameter that can be in the range 0.1 to 1.0.[8] (For a recent discussion about modelling this force see Ref. [9].)

Figure 6 shows that, like the lift force, a variation of the turbulent dispersion force modifies the gas volume fraction over the whole height but the slope of the curve does not change as much as when the lift force coefficient is varied.

4.3 Sato model

The Sato model takes into account the increment in the turbulence of the continuous phase induced by the dispersed phase. Denoting the continuous phase by α and the dispersed phase by β, the effective viscosity of the continuous phase is given by

$$\mu_{\alpha eff} = \mu_\alpha + \mu_{T\alpha} + \mu_{T\beta} \ . \tag{21}$$

The extra bubble induced turbulence term $\mu_{T\beta}$ is modelled by

$$\mu_{T\beta} = C_{\mu b} \rho_\alpha r_\beta d \, |\mathbf{U}_\beta - \mathbf{U}_\alpha| \ , \tag{22}$$

where d is the bubble diameter and $C_{\mu b}$ a constant usually equal to 0.6. The k and ε equations are solved only for the continuous phase and the effective viscosity of the dispersed phase is given as

$$\mu_{\beta eff} = \mu_{\alpha eff} \frac{\rho_\beta}{\rho_\alpha} \ . \tag{23}$$

As observed in figure 7 the influence of this effect is in the region near the nozzle, where gas fraction and relative velocity are greater.

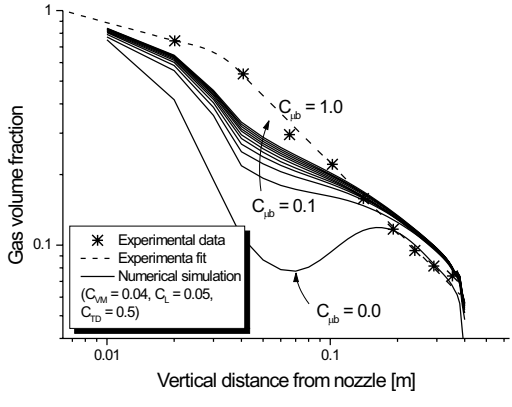

Figure 7: Axial gas fractions for different Sato coefficients

4.4 Influence of bubble size

The more difficult region to be correctly described is the region near the nozzle. In this region, bubbles are large and breakup and coalescence phenomena are important. As we mentioned before, a good modelling of this effect is complicated and since our primary interest is not in this region but in the region in which the plume is completely developed, we work with just one bubble size to represent the gas.

Ref. 2 gives us a geometric mean diameter of bubbles. Usually, the volumetric mean diameter is used to describe the interphase forces. However, in some cases the Sauter (or volume-surface) mean diameter[10] is also used because the quotient between the projected area and the volume of the bubble appears in the derivation of the drag force.

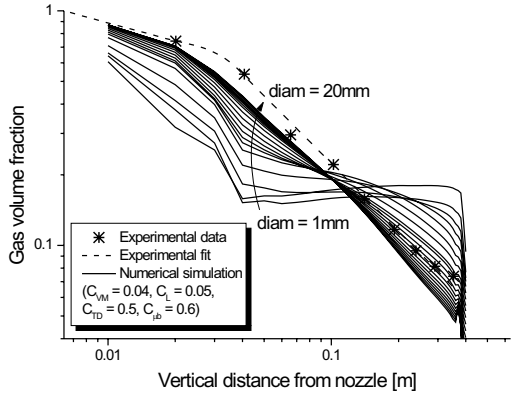

Figure 8: Axial gas fractions for different bubble diameters

Since there is not a unique criteria about which diameter should be used to represent the bubble size distribution, we analyzed the sensitivity to variations in diameter. Figure 8 shows how the volume fraction is modified when the diameter is varied. From this figure, it can be seen that when the same bubble size is used for all forces (drag and non-drag), the results are better when the volumetric mean diameter is used (which in this case is 16mm).

5 ANALYSIS OF DIFFERENT AIR-WATER PLUMES

After taking into account how the different parameters modify the numerical results, a better description of the system can be obtained. This is showed in figure 9 where preliminary (fig. 3) and optimized results are compared.

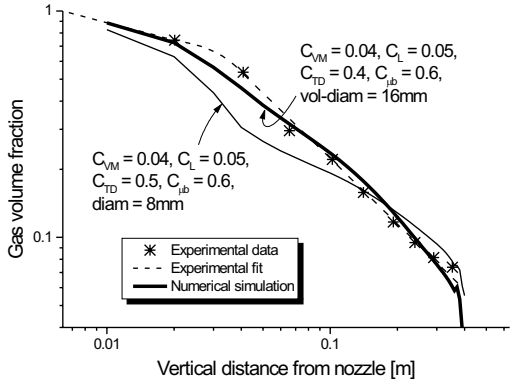

Figure 9: Axial gas fractions with optimized parameters

From an experimental point of view the system does not suffer substantial modifications in its behavior when the gas flow rate, the nozzle diameter or bath depth are changed (see fig. 5 of Ref. [2]) . So, it could be expected that the same coefficients of the non-drag forces are good in all cases. Our results indicate that this is not the case when only one bubble size is used. However, even with this restriction, a knowledge of the influence of the non-drag forces on the gas volume fraction allows a good description of the behavior of the system in all cases. For example, figure 10 shows a case where the experimental conditions are the same as those of figure 3 but with a higher gas flow rate ($1257\,\mathrm{cm}^3/\mathrm{s}$ at STP). Curve (a) is the result of using the parameters of figure 9 and curve (b) was obtained by modifying only the lift and the turbulent dispersion force coefficients.

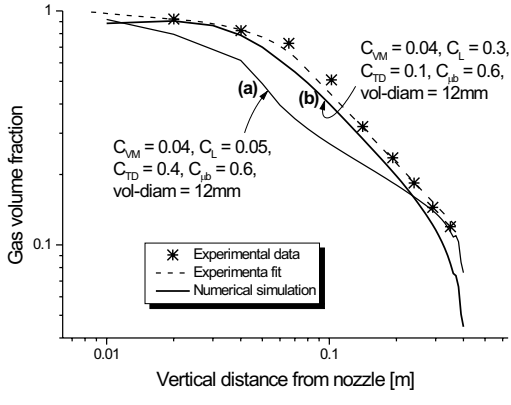

Figure 10: Axial gas fractions with optimized parameters for a case with a high gas flow rate

6 DEFORMABLE FREE SURFACE AND THREE-PHASE SYSTEM

In order to obtain a more realistic description of a metallurgical ladle two more ingredients have to be included. One of them is the treatment of the free surface and the other is the inclusion of the slag in the simulation.

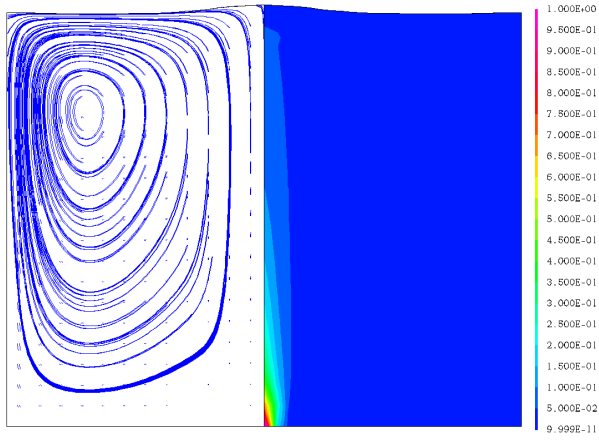

Figure 11: Streak lines (left) and volume fraction (right) when the free surface is deformable.

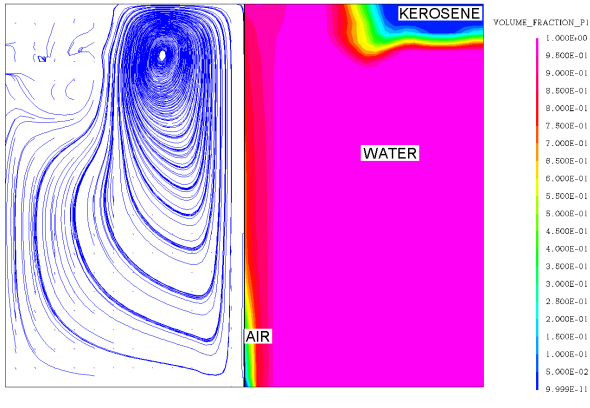

Figure 12: Streak lines (left) and volume fraction (right) corresponding to the water phase when coexists with the kerosene and the air phases.

Figure 11 shows how the free surface is deformed. Our results indicate that in the water-air system the consideration of the free surface as deformable does not modify substantially the solutions and a flat surface is a good approximation. In a graph as that of figure 9, gas volume fractions with and without free surface are practically indistinguishable.

When the slag is included (we simulate a water-air-kerosene system) the velocity field of the water is substantially modified as can be seen if we compare figure 1 with figure 12. Therefore, in order to make reasonable predictions about a real industrial ladle, consideration of a three-phase system is unavoidable.

7 CONCLUSIONS

If we are interested not only in the continuous phase but also in the behavior of the dispersed phases (gas or slag) in a gas stirred ladle, the effect produced by forces other than drag cannot be neglected.

In this work we make a detailed analysis of how the gas fraction is modified when non-drag effects are included. Our results indicate that the system can be described correctly in a wide variety of conditions using a simplified model with a unique bubble size, by adjusting a few parameters, such as lift and turbulent dispersion coefficients.

We also showed that the assumption of a flat free surface is a good approximation which can be used with confidence. Preliminary results indicate that if we want to obtain realistic values of the important variables in a real industrial metallurgical ladle, the consideration of a three-phase system (gas, molten metal and slag) is mandatory.

REFERENCES

[1] D. Mazumdar and R. I. L. Guthrie. *ISIJ Int.*, **35**, 1–20 (1995).
[2] A. H. Castillejos and J. K. Brimacombe. *Metall. Trans.*, **18B**, 659–671 (1987).
[3] M. Ishii. *Thermo-fluid dynamic theory of two-phase flow.* Eyrolles, Paris, (1975).
[4] L. Schiller and A. Nauman. *VDI Zeits.*, **77**, 318 (1933).
[5] A. Tomiyama. *Third International Conference on Multiphase Flow, ICMF'98, Lyon, France*, (1998).
[6] J. Hua and C. H. Wang. *Chem. Eng. Science*, **55**, 4159 (2000).
[7] M. Lopez de Bertodano. *Turbulent Bubbly Two-Phase Flow in a Triangular Duct.* Ph.D. thesis. Renssealaer Polytechnic Institute. Troy. New York, (1991).
[8] R. T. Jr. Lahey and D. A. Drew. *Japan/US Seminar on Two-Phase Flow Dynamics, Santa Barbara, California*, (2000).
[9] D. A. Drew F. J. Moraga, A. E. Larreteguy and R. T. Lahey Jr. *preprint*, (2001).
[10] R. S. Brodkey. *The Phenomena of Fluid Motions.* Publ. Co., Readin, MA, (1967).
[11] D. A. Drew and S. L. Passman. *Theory of Multicomponet Fluids.* Springer, (1999).